A computer simulation study of multiphase squeezing flows

Jonghoon Lee and Anthony J. C. Ladd[a)]
Chemical Engineering Department, University of Florida, Gainesville, Florida 32611-6005

(Received 2 October 2001; accepted 24 January 2002; published 19 March 2002)

The rheology of dense colloidal suspensions is sensitive to modifications in the surface properties of the particles. We are using lattice Boltzmann simulations to investigate the effects of polymer coatings on the squeezing flow between parallel plates. In this study, we used random arrays of stationary and mobile particles as the simplest models of the polymer coat. We have calculated the flow field in the gap and the force between the plates, and have compared the simulation results with analytic solutions based on the Stokes and Brinkman equations. Our models span the limiting characteristics of a polymer coated layer; namely a viscous suspension and a porous medium. We find good agreement between simulations and analytic solutions, even when the coat thickness is only a few Brinkman screening lengths. © *2002 American Institute of Physics.*
[DOI: 10.1063/1.1461372]

I. INTRODUCTION

Hydrodynamic interactions in colloidal suspensions give rise to frequency-dependent rheological properties on time scales that are experimentally and industrially relevant. Dimensional analysis of the hydrodynamic interactions implies that the relative viscosity of a suspension of hard spheres is a function of the volume fraction, ϕ, and Peclet number, Pe, only. It is composed of a frequency-independent hydrodynamic stress, coming from the added resistance to shear caused by fluid flow around the particles, and a frequency-dependent Brownian stress arising from viscous resistance to changes in particle position. Under a steady external shear rate, the suspension first exhibits shear thinning,[1] caused by a reduction in Brownian stress, which culminates in a second Newtonian region at a Peclet number, $\mathrm{Pe}=\gamma a^2/D$, around 10. Here we have defined the Peclet number as the product of the external shear rate, γ, and the diffusional relaxation time, a^2/D, for particles of radius a and diffusivity D. At Peclet numbers larger than 100, the effects of Brownian motion are small and the microstructure of the suspension is determined by the external shear rate. At high shear rates the hydrodynamic stress increases rapidly due to clustering of particles into transient aggregates, so that the stress tensor is dominated by the lubrication forces between particle surfaces close to contact.[2,3] It has been shown that the high-shear-rate behavior of a hard-sphere suspension is singular,[4] in that the viscosity increases without bound as the shear rate increases. The breakdown of this singular behavior is controlled by small additional effects, such as short-range repulsive forces, which inhibit cluster formation.[4–6] Thus minor modifications to the hydrodynamic flow field near the particle surface can produce substantial reductions in viscosity. Although this has been long known as an empirical fact, these recent simulation studies suggest the dominant mechanism is a microstructural rearrangement rather than a direct reduction in stress. The porous nature of the polymer coat reduces the singularity of the lubrication interaction, which prevents the build up of large transient aggregates of particles. As a consequence of this new understanding there is a strong motivation to understand the microstructural and rheological consequences of modifications to particle surface properties caused by coating them with polymers or polyelectrolytes. We plan to use numerical simulations to investigate the hydrodynamic interactions between surfaces coated with polymers and polyelectrolytes. However, in this work our aim is to assess the accuracy of the Brinkman equation as a model for the hydrodynamics in a porous coated surface driven by a squeezing flow between two parallel plates.

A phenomenological continuum description of the polymer phase has been widely adopted in theoretical[7] and numerical[8] approaches to calculating the lubrication forces between coated surfaces. Typically, the polymer phase is assumed to be a porous medium with a hydrodynamic screening length, ξ, determined by the local polymer concentration. A polymer in semidilute solution in a good solvent has a well-defined scaling relation between the hydrodynamic screening length, ξ, and the monomer concentration, c.[7,9] This description is based upon two assumptions. One is that the polymer phase is highly entangled. Thus individual chains (in semidilute solution) show Zimm dynamics on short length scales and Rouse dynamics on length scales larger than the screening length *for all times*.[10,11] The other assumption is that the hydrodynamic flow in the gap between the particles only varies significantly on length scales larger than the screening length. These two assumptions lead to a frequency-independent lubrication force, which can be calculated by assuming that the polymer layer can be treated as a porous medium, with a screening length ξ.

However, recent numerical simulations of semidilute polymer solutions show that there is a time dependence to the hydrodynamic screening of polymer chains that is neglected in the classical picture.[12] The simulations, which included hydrodynamic interactions,[12,13] showed a transition

a)Electronic mail: ladd@che.ufl.edu (URL:http://ladd.che.ufl.edu)

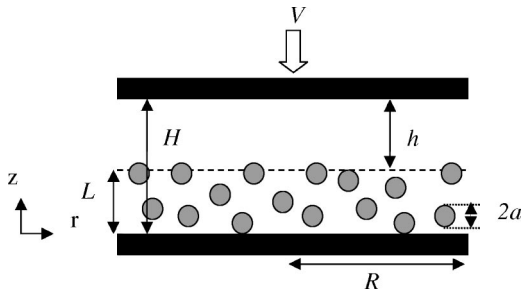

FIG. 1. Sketch of the geometry used in the simulation. The figure is a side view of a squeezing flow geometry using two flat disks of radius *R*, separated by a distance, *H*. The upper surface is moving downwards with a velocity *V*. The lower surface is stationary and coated with a suspension of either fixed or mobile beads of radius *a*. The thickness of the coat is *L*.

from Zimm-type to Rouse-type dynamics over the Zimm relaxation time of a blob, τ_Z. Thus for times shorter than the Zimm time, the single-chain dynamics is Zimm-type, independent of the length scale, which is in accordance with dynamic light scattering data.[14] This idea brings a subtle change to the phenomenological continuum picture of the polymer phase, from a rigid porous medium to a viscoelastic gel in which screening arises from the restricted mobility of the polymer chains due to the highly entangled structure. From the onset of the flow until the Zimm time the polymer phase acts as a viscous medium, but at longer times the individual beads cannot follow the flow due to the temporary structural hindrance, and therefore produces the screening characteristic of a rigid porous medium.[13,15] This picture suggests a qualitative dynamical change in the lubrication force between polymer coated surfaces over the time in which the polymer chains become entangled (Zimm time). We expect that constitutive equations describing the macrohydrodynamics of the system would show a time dependent change, from Stokes flow with an effective viscosity, to Darcy flow with an effective permeability.

Following this idea we present a preliminary computer simulation study of the lubrication force between two surfaces coated with model phases that characterize the macroscopic hydrodynamic interactions of a semidilute polymer solution. The model coat is composed of rigid spheres suspended in a viscous fluid and sandwiched between two flat circular plates (Fig. 1). The viscous or porous nature of the polymer phase can be modeled in an idealized fashion through the dynamics of the suspended spheres. If the spheres in the coat are fixed in position, the coat acts as a rigid porous medium producing Darcy friction, but if the spheres adjust their velocities to eliminate the drag caused by the local flow field, the coat acts as a viscous medium.

The Brinkman equation[16] has been proposed as a method for matching Darcy flow in a porous medium with Stokes flow in an adjacent volume. It has also been shown to be a good approximation of the flow in a porous medium driven by an external force.[17] In describing the flow in mixed porous and fluid phases the Brinkman equation is more satisfactory than a slip boundary condition at the interface between the porous and fluid phases, which requires an extra parameter to define the slip at the interface.[18] The Brinkman equation has been tested for pressure-driven flows in periodic porous media where exact solutions are available.[19,20] It was found that the agreement between the Brinkman equation and the exact solutions was reasonable if the porous medium was isotropic, but was quite poor if the medium was anisotropic. In view of this uncertainty and the widespread use of the Brinkman equation in modeling the hydrodynamic forces between polymer-coated particles, we have used a lattice-Boltzmann model of the fluid phase to carry out explicit simulations of fluid flow being squeezed out through gaps coated with permeable and viscous layers. We have compared the results of the simulations with analytic predictions based on continuum theories typically used to describe fluid flow in polymer coats.

II. THEORY

At the microscopic level, fluid flow is described by the Stokes equations

$$\nabla \cdot \mathbf{v} = 0, \quad \eta \nabla^2 \mathbf{v} = \nabla p, \tag{1}$$

and the coating is modeled by a random array of spherical beads, which interact with the fluid via a stick boundary condition on the particle surfaces. If the particles are free to move then the corresponding macroscopic equation for the flow of coating suspension is again Stokes flow, but with the viscosity now being the effective viscosity of the suspension. For simplicity we have assumed that the flow is sufficiently slow that the particles do not adjust their configuration over the duration of the numerical experiment. This enables us to keep the particles fixed in space while allowing their velocities to come to steady state with the fluid motion. The corresponding viscosity for this suspension is the high-frequency viscosity, $\eta_\infty(\phi)$, which has been accurately calculated in previous simulations.[2,4,21] We use a simple analytic expression, known to reproduce the simulation data for $\eta_r = \eta_\infty(\phi)/\eta$ with high accuracy,[21]

$$\frac{\eta_r - 1}{\eta_r + \frac{3}{2}} = \phi + \phi^2 + \phi^3 - 2.3\phi^4. \tag{2}$$

A stick boundary condition is also enforced on the upper and lower surfaces of the confining cell. The lower plate was chosen to be stationary and the upper plate was given a squeezing velocity, V $[v_z(H) = -V]$. In the continuum model we assume that the system is radially homogeneous and of infinite extent in the radial direction. We further assume a step discontinuity at the suspension-fluid interface and match the velocity and stress of the two phases in this plane. The solution of this model for the flow field and force on the plates is given in Appendix B.

For fixed particles (zero velocity) the appropriate macroscopic equation is the Brinkman equation,[16]

$$\nabla \cdot \mathbf{v} = 0, \quad \nabla p = \eta \nabla^2 \mathbf{v} - \eta \xi^{-2} \mathbf{v}, \tag{3}$$

where the permeability $K = \xi^2$ is determined by independent numerical simulations of Darcy flow in random arrays of spheres.[22] The Brinkman equation interpolates between Stokes equation and Darcy's law, to account for the momentum absorbed by a porous matrix. On length scales smaller

than the Brinkman screening length, ξ, viscous forces balance the pressure gradient, as in the Stokes equations [Eq. (1)]. On the other hand, on length scales greater than ξ, the pressure gradient is balanced by the drag on the solid matrix. The momentum absorbed by the solid phase screens the hydrodynamic interactions on length scales larger than ξ, whereas in suspensions the hydrodynamic interactions are unscreened.[23]

Although the Brinkman equation can be solved self-consistently to obtain numerical values of $K(\phi)$,[16] these results are not quantitatively correct at volume fractions greater than about 5% (see Fig. 5). However, given the permeability as a function of volume fraction, the Brinkman equation can be solved for the geometry shown in Fig. 1, again matching velocity and stress at the interface between the porous matrix and the fluid; the results are given in Appendix C. We have used an exact solution of these equations for comparison with the computer simulations. These solutions allow for cases when the radius of the disk is comparable to the height, leading to a z-dependent pressure field and when the thickness of the porous coat is comparable to the screening length. However, in most situations the coat thickness is large compared with the screening length, which simplifies the solution. In this case we find two different regimes, depending on the ratio of the thickness of the fluid film to the screening length in the porous medium.

III. SIMULATION METHOD

We simulate a squeezing flow between two circular plates using a three-dimensional 18-velocity lattice-Boltzmann model[24,25] of a fluid contained in a cylindrical cell. Boundary conditions on the upper and lower surfaces were implemented using the bounce-back collision rule for moving walls.[25] The upper wall ($z=H$) is moving with a velocity $v_z=-V$ and the lower wall is stationary. Again we assume that the velocity is sufficiently small that the walls do not move appreciably over the time scale of the simulation (H is independent of time). Thus the upper boundary is held fixed in place, but is nevertheless a source of mass and momentum flowing into the fluid phase. Since the simulated system is of finite extent in the horizontal direction, we must impose boundary conditions on the radial outflow through the side walls of the bounding cylinder. To do this we implement constant velocity boundary conditions on the side walls of the cylinder, where the local velocity of each boundary node is determined by solving the macroscopic equations for the appropriate geometry. The macroscopic solutions are scaled by a numerical factor $\alpha=1+\epsilon$ so that the total mass outflow exactly balances the inflow across the upper surface; typically ϵ is smaller than 10^{-5}.

The method was validated by simulating the squeezing flow of an incompressible fluid between two flat plates. Figure 2 shows that the radial velocity is axially symmetric and proportional to r, despite the irregularities in the bounding surface caused by discrete lattice artifacts. Due to the simple parallel geometry of this simulation, the lubrication force on the upper surface is simply the surface integration of the thermodynamic pressure at the surface ($\partial_z v_z|_{z=0,H}=0$). In

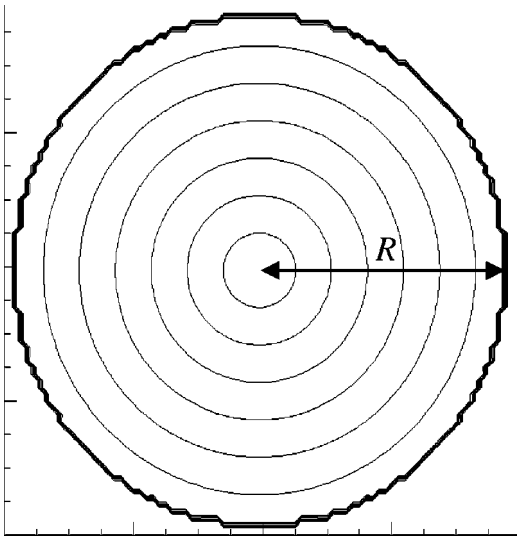

FIG. 2. Contour plot of the radial velocity field in the horizontal plane at $z=H/2$ for a single phase flow. The equally spaced contours show that the radial velocity increases linearly with the radial distance, which follows from the incompressibility of the flow. The smooth circles show that the effect of the pixelated outer surface do not penetrate into the flow.

lattice–Boltzmann simulations, the pressure at each node is calculated from the mass density $p=\rho c_s^2$, where the speed of sound (c_s) is dependent on the model parameters.[25] In these calculations $c_s=\sqrt{1/2}\Delta/\Delta t$, where Δ is the grid spacing and Δt is the time step of the lattice–Boltzmann model. The fluid nodes were located at half-integer positions, $\Delta/2, 3\Delta/2, \ldots, H-\Delta/2$, and the pressure was therefore extrapolated to the surfaces at $z=0$ and $z=H$. Since we implemented a constant velocity boundary condition on the side wall, the pressure in these simulations was undetermined to within an additive constant. As a reference, we took the pressure on the upper surface to be zero at the outer radial surface; i.e., $p(R,H)=0$.

The simulation results are compared with exact solutions of the Stokes equations in Figs. 3 and 4. For completeness the analytic solution is given in Appendix A. The simulated

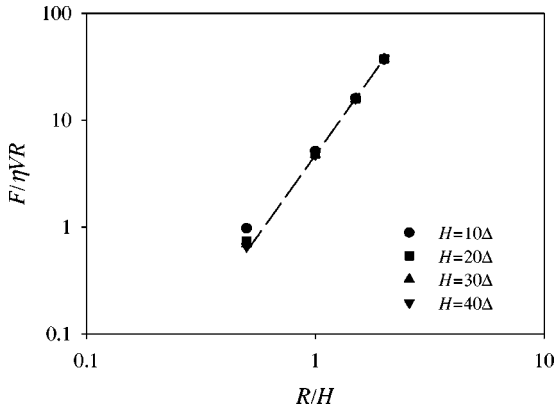

FIG. 3. Dimensionless lubrication force ($F/\eta VR$) as a function of the aspect ratio R/H for different heights. Analytic calculations indicates a power law dependence proportional to $(R/H)^3$ as indicated by the dotted line. The simulation results are within 1% of the analytic prediction when $R>1.5H$.

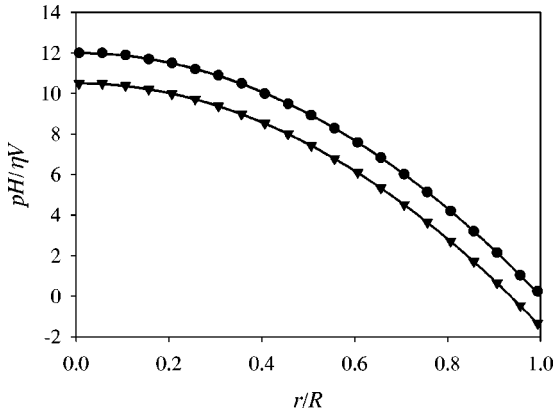

FIG. 4. Pressure profile in a squeezing flow ($H=40\Delta$, $R=80\Delta$). Lattice–Boltzmann simulations (solid symbols) are compared with analytic solutions of the Stokes equations (solid lines) at the upper ($z=H$, circles) and midplane ($z=H/2$, triangles) locations; the pressure on the upper surface and lower surface are identical. Note that there is a small but significant vertical variation in the pressure, which is ignored in the lubrication approximation. This variation vanishes in the limit $R \gg H$.

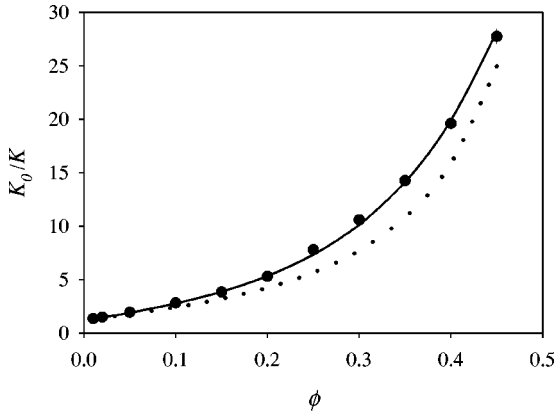

FIG. 5. Inverse permeability of a random array of solid spheres. Lattice–Boltzmann simulations (circles) are in good agreement with a precise multipole solution of the Stokes equations (solid line) (Ref. 21). The self-consistent solution of the Brinkman equation for the permeability is also shown (dotted line) (Ref. 16). The lattice–Boltzmann results are the average of ten independent configurations, and the resulting statistical errors are smaller than the size of the plotting symbols.

force on the upper and lower walls F is within 1% of the exact result,

$$\frac{F_0}{\eta V R} = \frac{3\pi}{2}\left(\frac{R}{H}\right)^3, \tag{4}$$

when $R/H \geqslant 1.5$ (Fig. 3). In the following simulations, R/H is always greater than 1.5. The calculated pressure field, shown in Fig. 4, is in perfect agreement with the analytic result given in Appendix A,

$$\frac{p(r,z)H}{\eta V} = 3\left(\frac{R}{H}\right)^2\left\{1-\left(\frac{r}{R}\right)^2\right\}+6\frac{z}{H}\left(\frac{z}{H}-1\right). \tag{5}$$

The lubrication approximation[7,26] ignores the dependence of the pressure on z, and is only valid when $R \gg H$.

The solid phase is introduced into the lattice Boltzmann fluid using the link bounce back collision rule.[22,25] We used small particles, with an input radius $a_0=2\Delta$, to maximize the number of particles in the coated layer while staying within the memory constraints imposed by our computer (500 MBytes). Despite the rather crude representation of the particle surface, previous work[22] has shown that hydrodynamic interactions between suspended spheres can be well described if the hydrodynamic radius of the particle is determined empirically. We used the sedimentation velocity of a single sphere in a periodic unit cell[22] with a solids volume fraction of 0.4% to determine the effective radius, $a=1.92\Delta$, which is used throughout this work.

Flow through a porous medium composed of randomly distributed spheres can be characterized by a permeability, K, relating the mean volumetric flow velocity U_V to the imposed pressure gradient,

$$\eta U_V = -K\nabla p. \tag{6}$$

To verify that the particles are large enough for the purposes of this study we have calculated the permeability $K(\phi)$ and compared the results with independent numerical solutions of high accuracy, obtained using a multipole expansion of the Stokes equations.[21] Owing to the screening of the long-range hydrodynamic interactions, periodic unit cells containing from 16 to 45 beads are sufficient to calculate the permeability.[21] Results for the inverse permeability K_0/K, scaled by the low density limit $K_0=\frac{2}{9}a^2\phi^{-1}$, are shown in Fig. 5. The results show that the lattice–Boltzmann simulations are in perfect agreement with the multipole results for all solids volume fractions up to 45%.

The numerical experiments described in this work were carried out over a range of volume fractions, from 0.5% to 45%. We have found that the results do not depend on volume fraction, except through the effect on the permeability. Thus all results are presented in terms of the Brinkman screening length $\xi=\sqrt{K}$ of the medium.

IV. RESULTS

A colloidal suspension of polymer-coated particles has three characteristic time scales: the time scale for the development of hydrodynamic interactions on the scale of the colloidal particles, $\tau_H=\rho a^2/\eta$, where ρ is the density of the solvent, which is also the relaxation time for the particle velocity $m/\eta a \sim \rho a^2/\eta$; the entanglement (Zimm) time of the polymer blob $\tau_Z=l_B^2/D_B=\eta l_B^3/k_BT$, where l_B and D_B are the size and the diffusivity of the blob; and the diffusion time for particle motion $\tau_P=a^2/D=\eta a^3/k_BT$. For a typical case of 1 μm particles and a 10 nm blob size, the time scales are $\tau_H \sim 1$ μs, $\tau_Z \sim 10$ μs, and $\tau_P \sim 1$ s. On the time scale for particle diffusion, the polymer phase will be entangled and thus behave hydrodynamically as a porous medium, but on the time scale of the relaxation of the colloidal particle velocity we may see the effect of the transition of the blob dynamics from mobile to entangled. However, experimental attempts have not yet been successful in observing frequency-dependent lubrication forces.[27,28] In this paper we have focused on squeezing flow in three different situations: a viscous layer filling a portion of the gap between the surfaces, a fixed porous layer filling a portion of the gap, and a

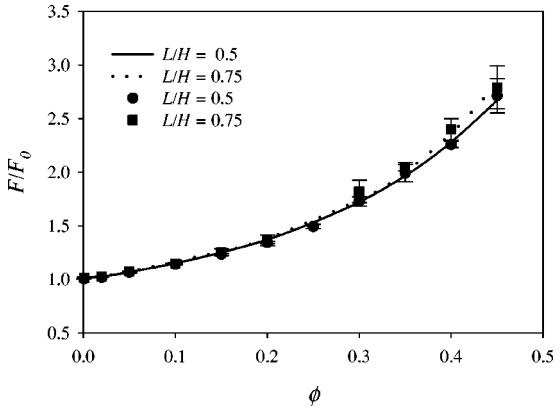

FIG. 6. Lubrication force for immiscible viscous fluids in a system of height $H=50\Delta$ and $R=75\Delta$. Lattice–Boltzmann simulations of the lubrication force (symbols) are compared with theoretical calculations based on the Stokes equations using the high-frequency viscosity, $\eta_\infty(\phi)$ for each region (see text).

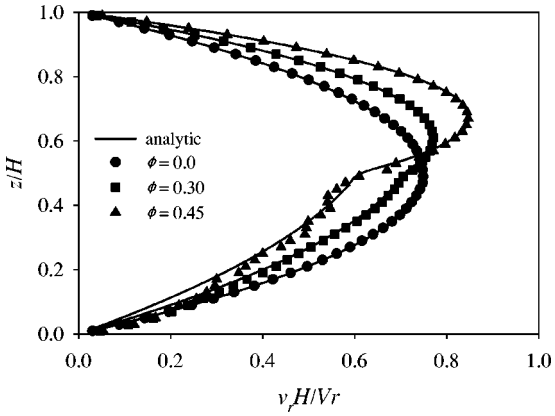

FIG. 7. Radial flow field for a two-phase viscous flow ($L/H=0.5$). The dimensionless radial velocity $v_r(r,z)H/Vr$ was averaged over radial direction and plotted as a function of z. For a radially homogeneous incompressible flow $v_r \propto r$. Lattice–Boltzmann results at different volume fractions (solid symbols) are compared with analytic solutions (solid lines) using the effective viscosity of the medium (Ref. 21).

fixed porous layer completely filling the gap. This last case corresponds to two coated layers compressed together. In all cases we have used random configurations of hard spheres, sampled from an equilibrium (most probable) distribution, and cut as sharply as possible along a horizontal plane, $z=L$, where L is the thickness of the coat. In the continuum models we have used a step function at $z=L$ for the particle-density profile.

A. Squeezing flow over a viscous coat of height, $L \leqslant H$

At short times ($\tau_H < t < \tau_Z$) the polymer coat behaves as a viscous medium, because, although the hydrodynamic flow is disturbed by the polymer phase, the screening mechanism caused by the restricted mobility of the blobs is not yet operative. As a simple model of this system, we used a random array of mobile non-Brownian beads. The beads adjust their velocities to eliminate the drag force from the surrounding flow, but their velocities are sufficiently small that they do not move a significant fraction of their radius during the course of the experiment. The macroscopic property characterizing the hydrodynamics of this medium is the high-frequency shear viscosity $\eta_\infty(\phi)$.

A squeezing flow was simulated with a viscous suspension coating the lower surface (Fig. 1), and the force on the upper surface and the radial flow field were measured. We also solved the Stokes equations at the macroscopic level, using appropriate viscosities for the pure solvent (η) and the suspension (η_∞), and coupling the two regions by a slip boundary condition at the solvent-suspension interface (see Appendix B). The flow fields and forces were then compared with the numerical data.

The lubrication force (Fig. 6) and the radial velocity field (Fig. 7) measured in the lattice Boltzmann simulations were in good agreement with the theoretical calculations, which assume that the coated layer behaves as a macroscopic viscous fluid. The small discrepancies in the flow field in the region near the lower plate are most likely the result of a technical problem with the computer program (now corrected), which prevented moving particles from approaching too close to the wall. Thus in these simulations there was a thin (0.5Δ) layer of pure fluid adjacent to the lower wall. This problem does not occur for stationary particles and for a porous layer of fixed particles the flow fields match very well (see Fig. 9).

B. Squeezing flow over a porous coat of height, $L \leqslant H$

At intermediate times ($\tau_Z < t < \tau_P$) the mobility of polymer chains are restricted by the entangled conformations. The polymer chains cannot follow the flow and the resulting fixed polymer matrix acts as a porous medium, screening the hydrodynamic interactions. Since the relaxation of the blob configuration only requires movement on the scale of the blob (10 nm), the change in the concentration profile of the polymer phase can be assumed to be negligible. Thus, we assume that the entangled polymer phase behaves as a rigid porous medium with permeability $K(\phi)=\xi^2$. We have again taken a random array of beads of thickness L to simulate the coating, but this time the particles are fixed in place, leading to a Darcy flow within the porous layer. For the purposes of the macroscopic calculation we assumed that the coating was a homogeneous distribution of particles with an isotropic screening length. The hydrodynamic flow fields and lubrication forces were calculated by solving the Brinkman equation for the porous medium and Stokes equation for the pure solvent region, with a slip boundary condition at the interface (see Appendix C).

The simulated lubrication force and the radial velocity field are compared with the Brinkman model in Figs. 8 and 9. Lubrication forces (Fig. 8) are in good agreement with the Brinkman model (solid lines) over a broad range of screening length, ξ/L, and for different values of coat thicknesses, H/L. The flow fields calculated macroscopically and microscopically are in excellent agreement overall (Fig. 9), both for cases when the coat thickness is a few screening lengths and the flow fields penetrates deeply into the porous coat, and when the screening length is very short and the coat

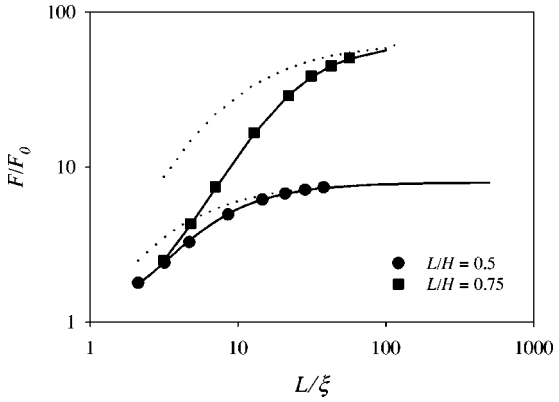

FIG. 8. Lubrication force for an uncompressed porous layer ($L<H$) for a system of height $H=50\Delta$ and $R=75\Delta$. Lattice–Boltzmann simulations of the lubrication force (symbols) are compared with theoretical calculations based on the Brinkman equation (solid lines). F_0 is the lubrication force of the pure fluid layer ($L=0$). The two asymptotes (dotted lines) are based on the limit $l_p=\xi$ in Eq. (7). Each symbol is the average of five independent configurations; the statistical errors are smaller than the size of symbols.

behaves as a nearly impermeable layer with large velocity gradients near the interface. However, at high volume fractions ($\xi<a$) there are small but noticeable deviations near the interface, which is most likely a manifestation of the fact that the screening length is significantly smaller than the particle radius. It should be noted that the coatings are always at least $10a$ thick; the long screening lengths ($\xi/a\sim10$) were obtained using dilute suspensions.

When $L<H$ the two-phase medium between the surfaces is heterogeneous at the macroscopic length scale and cannot be characterized by the screening length alone. Instead, the effect of the surface heterogeneity on the hydrodynamics is often represented by an empirical ''hydrodynamic thickness (L_H)'' of the porous medium or equivalently the ''penetration depth ($l_p=L-L_H$)'' of the flow field into the porous medium.[29] These are measures of the apparent location of the no-slip boundary inside the porous medium, assuming the expression for the lubrication force is similar to the pure fluid case

$$\frac{F}{F_0}=\left(\frac{H}{H-L_H}\right)^3=\left(\frac{H}{H-L+l_p}\right)^3=\left(\frac{H}{h+l_p}\right)^3, \tag{7}$$

where F_0 is the lubrication force in the absence of the coat ($L=0$) and $h=H-L$.

Though the expression given in Eq. (7) is simple, the location of the no-slip boundary is not always a well-defined material property. Examples of experimental techniques for measuring the hydrodynamic thickness of the polymer coat are the reduction of solvent flux in a flow channel,[30] or the increase in the drag coefficient of a colloidal particle upon adsorption of a polymer phase onto the surface.[31,32] Theoretical treatments of the hydrodynamic thickness[29,33] have assumed that the flow fields in the vicinity of the polymer phase is simple shear, and then determined the location of the apparent no-slip boundary, based on the velocity gradient at the interface between the polymer phase and the solvent phase

$$l_p=\left(\frac{v_r}{\partial_z v_r}\right)_{z=L}. \tag{8}$$

In a simple shear flow, when the density profile of the polymer phase is a step function, the porous medium screens the hydrodynamic interactions with an isotropic length scale of ξ. Thus the solution to Eq. (8) is simply $l_p=\xi$. However, in a squeezing flow, the penetration depth must be deeper than in a pure shear flow, due to the presence of the pressure gradient. Thus the hydrodynamic thickness (L_H) of the polymer phase does not describe the location of the plane where the velocity field actually vanishes but rather the phenomenological effect of the coat on the macroscopic hydrodynamics.

The apparent location of the no-slip boundary can be determined theoretically by matching the solution of the lubrication force [Eq. (C11)] with that for the pure solvent [Eq. (A6)].[27] We can obtain an analytic expression for the hydrodynamic thickness from the solution of the Brinkman model (see Appendix C),

$$L_H=L-l_p=\left\{1-\left(\frac{2}{\alpha}\right)^{1/3}\right\}H, \tag{9}$$

where

$$\alpha=\frac{2}{3}\left(\frac{H}{R}\right)^2\frac{Hp(0,H)}{\eta V}. \tag{10}$$

The actual expression for α (or equivalently the dimensionless pressure, $p(0,H)H/\eta V$) is a complex function of L/H and ξ/H [see Appendix C, Eqs. (C17) and (C18)].

Figure 10 shows the simulated penetration length, calculated from the lubrication force measured in the lattice Boltzmann simulations, and compares them with Eq. (9). Penetration lengths based on the gradient of the radial velocity at the interface [Eq. (8)] are also shown. In the radial direction, the squeezing flow inside the porous medium has a driving force from the pressure gradient in addition to the momen-

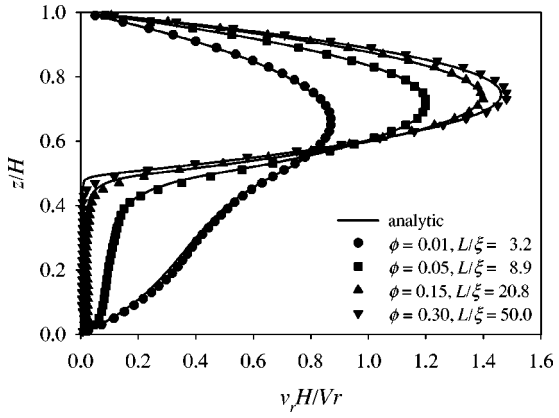

FIG. 9. Radial flow field for a squeezing flow including a porous matrix ($L/H=0.5$). The dimensionless radial velocity $v_r(r,z)H/Vr$ was averaged over radial direction and plotted as a function of z. Lattice–Boltzmann results for different screening lengths (solid symbols) are compared with analytic solutions (solid lines) using the effective permeability of the medium $K=\xi^2$ (see Appendix C).

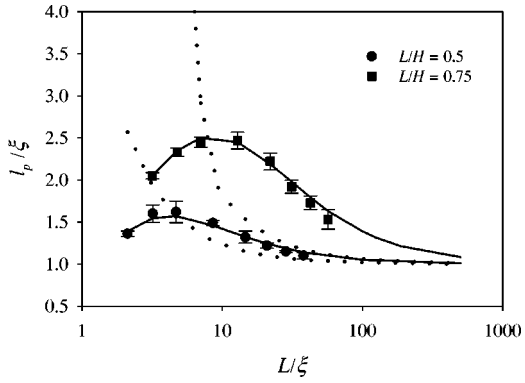

FIG. 10. Penetration depth of a squeezing flow. The penetration depth l_p has been determined by fitting the simulated force to Eq. (7). The solid lines are calculated by an analytic solution of the Brinkman equation [Eq. (9)] for coat thicknesses $L/H=0.5$ and $L/H=0.75$. The dotted line is calculated based on the velocity gradient at the interface [Eq. (8)]. The penetration depth is a function only of the scaled height H/ξ and coat thickness L/ξ. At large values of H/ξ, the penetration depth based on the lubrication force is identical to that based on the velocity gradient, but for small gaps it is much smaller.

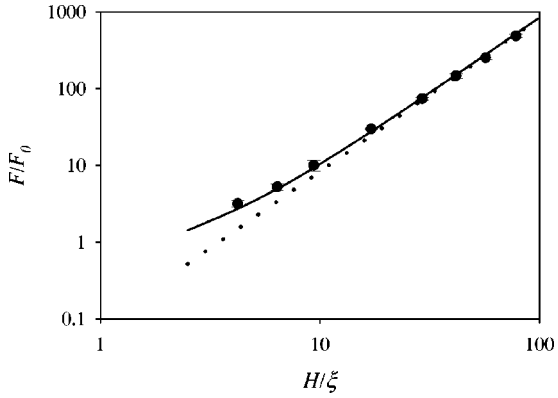

FIG. 11. Lubrication force for a compressed porous coat ($L=H$), with $L=50\Delta$ and $R=75\Delta$. Lattice–Boltzmann simulations (symbols) of the lubrication force are compared with the Brinkman model. The $H/\xi \gg 1$ asymptote (dashed line) is from Eq. (12).

tum transferred from the pure solvent region as shear stress. As L/ξ decreases, the effect of the pressure gradient becomes dominant and makes the penetration length based on Eq. (8) diverge. However, when the coat thickness is large compared to the screening length ($L/\xi \gg 1$), both penetration lengths approach the screening length.

C. Squeezing flow over a full porous coat, $L=H$

When $L=H$, the medium can be regarded as homogeneous and isotropic on the macroscopic length scale and the lubrication force is now a universal function of H/ξ where ξ is the screening length that characterizes the medium. The solution to Brinkman's equation (Appendix C),

$$\frac{F}{\eta V R}=\frac{3\pi\alpha}{4}\left(\frac{R}{H}\right)^3, \tag{11}$$

shows that the lubrication force has simple asymptotic power law dependence on H/ξ when $H \gg \xi$,

$$\frac{F}{F_0}=\frac{1}{12}\left(\frac{H}{\xi}\right)^2. \tag{12}$$

In Fig. 11, the lubrication forces measured using lattice Boltzmann simulations are compared with the analytic solution to the Brinkman's equation. Several different volume fractions were used to give a range of screening lengths. The quadratic dependence of F/F_0 on H/ξ in the limit $H/\xi \gg 1$ was predicted earlier.[7,26] It can be seen from Figs. 8 and 11 that the Brinkman equation is valid at surprisingly small values of L/ξ, even though there are noticeable deviations from the asymptotic behavior. Our results suggest that a continuum description is quantitatively correct for both the force and the radial flow field, even when the macroscopic coat thickness is only a few screening lengths.

D. Squeezing flow between two coated surfaces, $L \gg \xi$

The numerical simulations used only a single coated surface, to maximize the thickness of the porous coat in terms of the particle radius ($L>10a$), thus avoiding artifacts due to an additional length scale (a). Here we examine the flow between two coated surfaces, separated by a distance H, in the limit that the coating thickness L is large compared with the screening length ξ. The force can be expressed in an analogous form to Eq. (7)

$$\frac{F}{F_0}=\left(\frac{H}{h+2l_p}\right)^3, \tag{13}$$

where the factor of 2 comes from the penetration of the flow into each coat. When $\exp(L/\xi) \gg 1$, we obtain a relatively simple expression for the penetration length (see Appendix D),

$$\frac{h+2l_p}{h+2\xi}=\left(1+\frac{3x^3H}{2\xi}-4x^3\right)^{1/3}, \tag{14}$$

where $x=2\xi/(h+2\xi)$. If the fluid layer is sufficiently thick [and $\exp(L/\xi) \gg 1$], the penetration length $l_p=\xi$ is a genuine material property, identical for both shear flow and squeeze flow. As the gap between the surfaces decreases, the pressure gradient drives the flow deeper into the porous coats, to a depth that is no longer constant, but depends on $h/\xi=2(1-x)/x$. In the limit $h \to 0$ we again recover Eq. (12) for the lubrication force, but more significantly, Eq. (14) shows that the $h \to 0$ limit applies whenever the gap between the surfaces h is sufficiently small that $3x^3H/2\xi \gg 1$. Thus the penetration length diverges for small gaps ($h \ll \xi$), so long as the condition $\exp(L/\xi) \gg 1$ is maintained. In Fig. 10 the penetration length decreases because this condition is no longer met.

V. SUMMARY

In this work we have simulated a squeezing flow between surfaces coated with random arrays of small particles. These coatings are idealized models for the effects of an adsorbed polymer layer on the flow of a viscous fluid. The

properties of the coatings could be adjusted to model a viscous suspension (mobile particles) or a porous medium (fixed particles).

We found that macroscopic theories based on the Stokes and the Brinkman equations accurately reproduced the lubrication force and flow fields obtained by direct numerical simulation. The comparison of the Brinkman theory with the results of the numerical simulations did not involve any additional parameters; the viscosity in the porous medium was that of the pure fluid, and the screening length was determined from the bulk permeability, independently measured. The range of validity of the macroscopic equations was surprising; we obtained quantitatively accurate flow field even when the coat thickness was only 2 screening lengths. This work suggests that discrepancies between experimental measurement of the lubrication force[27] and theoretical calculations[7] lie in the polymer statistics rather than the hydrodynamic calculation, which is based on the Brinkman equation.

The penetration length, representing the effect of the coating on the hydrodynamic flow field, should be calculated from the lubrication force rather than the gradient of the radial velocity. We have found that the concept of penetration length is physically sensible only when both the porous coat and the fluid layer are thick compared with the screening length [$\exp(L/\xi) \gg 1$ and $h \gg \xi$]. When the fluid layer is of comparable thickness to the screening length, the important length scale is once again the gap between the plates. In this case the flow penetrates to the solid surfaces and the force depends only weakly on separation [cf. Eq. (4)],

$$\frac{F}{\eta V R} = \frac{\pi R^3}{8HK} \tag{15}$$

although it is amplified by the inverse permeability of the medium, K^{-1}. The calculations in Appendix D show that the transition region occurs when

$$\frac{h}{\xi} \approx \left(\frac{H}{\xi}\right)^{1/3}. \tag{16}$$

These results suggest that a permeable coat can substantially modify the lubrication forces in the region when the gap between the polymer coats is small [$h \approx (H\xi^2)^{1/3}$], but when polymers on different surfaces have not yet begun to repel each other strongly. This purely hydrodynamic effect is in addition to transitions caused by changes in polymer density as the surfaces approach.[26]

ACKNOWLEDGMENT

This work was supported in part by the National Science Foundation, via the Engineering Research Center for Particle Science and Technology at the University of Florida (EEC-94-02989).

APPENDIX A: SQUEEZING FLOW IN A SINGLE-PHASE FLUID

Consider two parallel disks of radius R, separated by H. The upper surface has a velocity $-V$ in the z direction, and the lower surface is stationary. The gap between the surfaces is filled with an incompressible viscous fluid. Scaling the velocity field ($\mathbf{v}$) by V, distances (r and z) by H, and the pressure (p) by $\eta V/H$, leads to the dimensionless Stokes equations,

$$\tilde{\nabla}\cdot\tilde{\mathbf{v}} = 0,\ \tilde{\nabla}^2\tilde{\mathbf{v}} = \tilde{\nabla}\tilde{p}. \tag{A1}$$

We assume that the normal velocity component, $\tilde{v}_z$, is independent of radial direction, which is equivalent to neglecting end effects and gains validity as R/H increases. Then the incompressibility condition leads to a radial velocity that is linear in the radial distance $\tilde{r}$,

$$\tilde{v}_z = \tilde{v}_z(\tilde{z}),\ \tilde{v}_r = -\frac{\tilde{r}}{2}\frac{d\tilde{v}_z}{d\tilde{z}}. \tag{A2}$$

With this form for the velocity field, the Stokes equations [Eq. (A1)] simplify to

$$\frac{\partial^2\tilde{p}}{\partial\tilde{r}\,\partial\tilde{z}} = -\frac{\tilde{r}}{2}\frac{d^4\tilde{v}_z}{d\tilde{z}^4} = 0, \tag{A3}$$

which requires $\tilde{v}_z$ to be a cubic polynomial in $\tilde{z}$,

$$\begin{aligned}\tilde{v}_z &= \alpha\tilde{z}^3 + \beta\tilde{z}^2 + \gamma\tilde{z} + \delta,\\ \tilde{v}_r &= -\frac{\tilde{r}}{2}(3\alpha\tilde{z}^2 + 2\beta\tilde{z} + \gamma).\end{aligned} \tag{A4}$$

The pressure can then be calculated, using $\tilde{p}(\tilde{R},1) = 0$ as a boundary condition to determine the integration constant,

$$\tilde{p} = \frac{3\alpha}{2}(-\tilde{r}^2 + \tilde{R}^2) + 3\alpha(\tilde{z}^2 - 1) + 2\beta(\tilde{z} - 1). \tag{A5}$$

The coefficients $\alpha = 2$, $\beta = -3$, $\gamma = \delta = 0$ are determined from the no-slip conditions at $\tilde{z} = 0$ and $\tilde{z} = 1$.

The lubrication force can be calculated by surface integration of the pressure. If we use the upper surface

$$\tilde{F} = \frac{F}{\eta V H} = \int_0^{\tilde{R}} d\tilde{r}\, 2\pi\tilde{r}\tilde{p}(\tilde{r},1) = \frac{3\pi\alpha}{4}\tilde{R}^4 = \frac{3\pi}{2}\tilde{R}^4, \tag{A6}$$

which leads to the standard expression for the lubrication force between parallel disks,[34]

$$\frac{F}{\eta V R} = \frac{3\pi}{2}\left(\frac{R}{H}\right)^3. \tag{A7}$$

APPENDIX B: SQUEEZING FLOW IN IMMISCIBLE FLUIDS

The geometry is the same as in the preceding section, but the gap between the plates is composed of two immiscible viscous fluids. The lower medium ($0 < z < L$) has a viscosity η' and the upper medium has a viscosity η. Scaling the pressure in each region by the appropriate viscosity, $\tilde{p} = pH/\eta V$ and $\tilde{p}' = p'H/\eta' V$, the Stokes equations for each region are

$$\begin{aligned}&\tilde{\nabla}\cdot\tilde{\mathbf{v}} = 0,\\ &\tilde{\nabla}\tilde{p} = \tilde{\nabla}^2\tilde{\mathbf{v}} \quad \text{for} \quad \tilde{L} < \tilde{z} < 1,\end{aligned} \tag{B1}$$

$$\tilde{\nabla}\tilde{p}' = \tilde{\nabla}^2\tilde{\mathbf{v}}' \quad \text{for} \quad 0<\tilde{z}<\tilde{L}.$$

The velocity and pressure in each region are the same as in Appendix A,

$$\tilde{v}_z = \alpha\tilde{z}^3 + \beta\tilde{z}^2 + \gamma\tilde{z} + \delta,$$
$$\tilde{v}_z' = \alpha'\tilde{z}^3 + \beta'\tilde{z}^2 + \gamma'\tilde{z} + \delta', \tag{B2}$$

$$\tilde{v}_r = -\frac{\tilde{r}}{2}(3\alpha\tilde{z}^2 + 2\beta\tilde{z} + \gamma),$$
$$\tilde{v}_r' = -\frac{\tilde{r}}{2}(3\alpha'\tilde{z}^2 + 2\beta'\tilde{z} + \gamma'), \tag{B3}$$

$$\tilde{p} = -\frac{3}{2}\alpha(\tilde{r}^2 - \tilde{R}^2) + 3\alpha(\tilde{z}^2 - 1) + 2\beta(\tilde{z} - 1),$$
$$\tilde{p}' = -\frac{3}{2}\alpha'(\tilde{r}^2 - \tilde{R}^2) + 3\alpha'\tilde{z}^2 + 2\beta'\tilde{z} + \text{const}. \tag{B4}$$

In the numerical simulations, the integral of the pressure over the volume of fluid is independent of velocity. We match this condition closely by the boundary condition $\tilde{p}(\tilde{R},1)=0$, which is used as an integration constant for $\tilde{p}$ in Eq. (B4). Neglecting end effects adds a constant to $\tilde{p}'$, which is determined by the stress matching condition at the interface ($\tilde{z}=\tilde{L}$). This additional pressure is due to the assumption that $\tilde{v}_z$ is independent of radial direction, and is negligible when $R/H \gg 1$.

The lubrication force can again be calculated by integrating the pressure on either surface,

$$\tilde{F} = \int_0^{\tilde{R}} d\tilde{r}\, 2\pi\tilde{r}\tilde{p}(\tilde{r},1) = \frac{3\pi\alpha}{4}\tilde{R}^4, \tag{B5}$$

as in Eq. (A6).

The boundary conditions for determining the coefficients in Eq. (B2) are no slip at $\tilde{z}=0$ and $\tilde{z}=1$, and continuity of velocity and stress along the interface ($\tilde{z}=\tilde{L}$). Since the equation for $\tilde{p}'$ [Eq. (B4)] has an undetermined constant, we match the radial gradient of pressure ($\partial\tilde{p}/\partial\tilde{r} = \partial\tilde{p}'/\partial\tilde{r}$) instead of the normal stress; the constant can be determined by also matching pressures at $\tilde{z}=\tilde{L}$. The boundary conditions can be simplified to conditions on $\tilde{v}_z$ and its derivatives using Eqs. (B2) and (B3),

$$\tilde{v}_z = -1, \quad \frac{d\tilde{v}_z}{d\tilde{z}} = 0 \quad \text{at} \quad \tilde{z}=1, \tag{B6}$$

$$\tilde{v}_z' = 0, \quad \frac{d\tilde{v}_z'}{d\tilde{z}} = 0 \quad \text{at} \quad \tilde{z}=0, \tag{B7}$$

$$\tilde{v}_z = \tilde{v}_z', \quad \frac{d\tilde{v}_z}{d\tilde{z}} = \frac{d\tilde{v}_z'}{d\tilde{z}}, \quad \eta\frac{d^2\tilde{v}_z}{d^2\tilde{z}} = \eta'\frac{d^2\tilde{v}_z'}{d^2\tilde{z}},$$
$$\eta\frac{d^3\tilde{v}_z}{d^3\tilde{z}} = \eta'\frac{d^3\tilde{v}_z'}{d^3\tilde{z}} \quad \text{at} \quad \tilde{z}=\tilde{L}. \tag{B8}$$

The coefficients calculated from these boundary conditions are

$$\alpha = \frac{2\tilde{L}(\eta_r^{-1}-1)+2}{\det[\mathbf{M}]}, \tag{B9}$$

$$\beta = -\frac{3\tilde{L}^2(\eta_r^{-1}-1)+3}{\det[\mathbf{M}]}, \tag{B10}$$

$$\gamma = -3\alpha - 2\beta, \tag{B11}$$

$$\delta = 2\alpha + \beta - 1, \tag{B12}$$

$$\alpha' = \eta_r^{-1}\alpha, \quad \beta' = \eta_r^{-1}\beta, \tag{B13}$$

$$\gamma' = 0, \quad \delta' = 0, \tag{B14}$$

where

$$\mathbf{M} = \begin{pmatrix} 3\tilde{L}^2(\eta_r^{-1}-1)+3 & 2\tilde{L}(\eta_r^{-1}-1)+2 \\ \tilde{L}^3(\eta_r^{-1}-1)+3\tilde{L}-2 & \tilde{L}^2(\eta_r^{-1}-1)+2\tilde{L}-1 \end{pmatrix}. \tag{B15}$$

APPENDIX C: SQUEEZING FLOW IN A BRINKMAN LAYER

The geometry of problem is the same as in Appendix B except that the coating is a porous medium with screening length, ξ.

Fluid flow in this system can be described by the Stokes equation in the upper region and the Brinkman equation for the flow in the lower porous region,

$$\tilde{\nabla}\cdot\tilde{\mathbf{v}} = 0, \tag{C1}$$

$$\tilde{\nabla}\tilde{p} = \tilde{\nabla}^2\tilde{\mathbf{v}} \quad \text{for } \tilde{L}<\tilde{z}<1, \tag{C2}$$

$$\tilde{\nabla}\tilde{p}' = -\frac{\tilde{\mathbf{v}}'}{\tilde{\xi}^2} + \tilde{\nabla}^2\tilde{\mathbf{v}}' \text{ for } 0<\tilde{z}<\tilde{L}. \tag{C3}$$

If we again neglect end effects, $\tilde{v}_z$ is independent of $\tilde{r}$, and $\partial^2\tilde{p}/\partial\tilde{r}\partial\tilde{z}=0$ for both the viscous and porous regions. Then, Eq. (C3) can be simplified to a fourth order differential equation for $\tilde{v}_z$,

$$\partial_{\tilde{z}}^4\tilde{v}_z' - \frac{\partial_{\tilde{z}}^2\tilde{v}_z'}{\tilde{\xi}^2} = 0. \tag{C4}$$

Velocity fields satisfying the no-slip boundary conditions at $\tilde{z}=0$ and 1 are,

$$\tilde{v}_z = \alpha\tilde{z}^3 + \beta\tilde{z}^2 - (3\alpha+2\beta)\tilde{z} + 2\alpha + \beta - 1, \tag{C5}$$

$$\tilde{v}_z' = ae^{\tilde{z}/\tilde{\xi}} + be^{-\tilde{z}/\tilde{\xi}} - \left(\frac{a-b}{\tilde{\xi}}\right)\tilde{z} - a - b, \tag{C6}$$

$$\tilde{v}_r = -\frac{\tilde{r}}{2}(3\alpha\tilde{z}^2 + 2\beta\tilde{z} - 3\alpha - 2\beta), \tag{C7}$$

$$\tilde{v}_r' = -\frac{\tilde{r}}{2\tilde{\xi}}(ae^{\tilde{z}/\tilde{\xi}} - be^{-\tilde{z}/\tilde{\xi}} - a + b), \tag{C8}$$

and Eq. (C2) and Eq. (C3) give pressure fields

$$\tilde{p} = -\tfrac{3}{2}\alpha(\tilde{r}^2 - \tilde{R}^2) + 3\alpha(\tilde{z}^2 - 1) + 2\beta(\tilde{z} - 1), \tag{C9}$$

$$\tilde{p}' = -\frac{a-b}{4\tilde{\xi}^3}(\tilde{r}^2 - \tilde{R}^2) + \frac{1}{\tilde{\xi}^2}\left\{\frac{a-b}{2\tilde{\xi}}\tilde{z}^2 + (a+b)\tilde{z}\right\} + \text{const}, \tag{C10}$$

where $\tilde{p}(\tilde{R},1) = 0$ is used as the boundary condition. The constant term in the equation for $\tilde{p}'$ can be determined by matching pressures at $\tilde{z} = \tilde{L}$.

The lubrication force can be again calculated from the surface integral of $\tilde{p}(\tilde{r},1)$ on the upper surface,

$$\tilde{F} = \frac{3\pi\alpha}{4}\tilde{R}^4, \tag{C11}$$

but the force on the lower surface also includes the force on the stationary particles composing the porous matrix. Comparing Eq. (C11) with Eq. (A7), the hydrodynamic thickness of the coat [see Eq. (7)] can also be calculated,

$$L_H = \left\{1 - \left(\frac{2}{\alpha}\right)^{1/3}\right\} H. \tag{C12}$$

The coefficients in Eqs. (C5) and (C6) are obtained by matching velocity, tangential velocity, and pressure (at $\tilde{z} = \tilde{L}$). Again we write the boundary conditions in terms of $\tilde{v}_z$ and its derivatives [see Eq. (B8)],

$$\tilde{v}_z = \tilde{v}_z', \tag{C13}$$

$$\frac{d\tilde{v}_z}{d\tilde{z}} = \frac{d\tilde{v}_z'}{d\tilde{z}}, \tag{C14}$$

$$\frac{d^2\tilde{v}_z}{d^2\tilde{z}} = \frac{d^2\tilde{v}_z'}{d^2\tilde{z}}, \tag{C15}$$

$$\frac{d^3\tilde{v}_z}{d^3\tilde{z}} = \frac{d^3\tilde{v}_z'}{d^3\tilde{z}} - \frac{1}{\tilde{\xi}^2}\frac{d\tilde{v}_z'}{d\tilde{v}_z'}. \tag{C16}$$

The coefficient of the pressure, α, is given by

$$\alpha = \frac{-2\tilde{\xi}\{e^{\tilde{L}/\tilde{\xi}}(\tilde{L} - \tilde{\xi} - 1) + e^{-\tilde{L}/\tilde{\xi}}(\tilde{L} + \tilde{\xi} - 1)\}}{\det[\mathbf{N}]}, \tag{C17}$$

where

$$\mathbf{N} = \begin{pmatrix} 3\tilde{\xi}(L_1 + 2\tilde{\xi}\tilde{L} + 2\tilde{\xi}^2) + e^{\tilde{L}/\tilde{\xi}}(L_2 - 6\tilde{\xi}^3) & 2\tilde{\xi}(L_3 + \tilde{\xi}) + e^{\tilde{L}/\tilde{\xi}}(L_4 - 2\tilde{\xi}^2) \\ -3\tilde{\xi}(L_1 - 2\tilde{\xi}\tilde{L} + 2\tilde{\xi}^2) + e^{-\tilde{L}/\tilde{\xi}}(L_2 + 6\tilde{\xi}^3) & -2\tilde{\xi}(L_3 - \tilde{\xi}) + e^{-\tilde{L}/\tilde{\xi}}(L_4 - 2\tilde{\xi}^2) \end{pmatrix}, \tag{C18}$$

$L_1 = \tilde{L}^2 - 1$, $L_2 = \tilde{L}^3 - 3\tilde{L} + 2$, $L_3 = \tilde{L} - 1$,

and

$L_4 = \tilde{L}^2 - 2\tilde{L} + 1$.

When the space between the surfaces is filled with the porous medium ($\tilde{L} = 1$), $L_1 = L_2 = L_3 = L_4 = 0$. In the limit $\tilde{L} \gg \tilde{\xi}$, α can be approximated by $(6\tilde{\xi}^2)^{-1}$, and Eq. (C11) becomes

$$\tilde{F} = \frac{F}{\eta V H} = \frac{\pi}{8}\frac{R^4}{\xi^2 H^2}, \tag{C19}$$

so that

$$\frac{F}{F_0} = \frac{1}{12}\left(\frac{H}{\xi}\right)^2. \tag{C20}$$

APPENDIX D: SQUEEZING FLOW BETWEEN TWO BRINKMAN LAYERS

The geometry is the same as in Appendix C, except that the upper boundary is now a mirror plane ($v_z = \partial v_r/\partial z = 0$), rather than a rigid wall. If we scale the length by $H/2$ rather than H, then the scaled equations are the same as in Appendix C. We consider that the walls are approaching each other with a relative velocity V, so that the z velocity on the lower wall is $V/2$.

Velocities satisfying the no-slip boundary condition at $\tilde{z} = 0$ and mirror symmetry in the plane $z = 1$ are

$$\tilde{v}_z = \alpha\tilde{z}^3 - 3\alpha\tilde{z}^2 + \gamma\tilde{z} + 2\alpha - \gamma, \tag{D1}$$

$$\tilde{v}_z' = ae^{\tilde{z}/\tilde{\xi}} + be^{-\tilde{z}/\tilde{\xi}} - \left(\frac{a-b}{\tilde{\xi}}\right)\tilde{z} - a - b + \frac{1}{2}, \tag{D2}$$

$$\tilde{v}_r = -\frac{\tilde{r}}{2}(3\alpha\tilde{z}^2 - 6\alpha\tilde{z} + \gamma), \tag{D3}$$

$$\tilde{v}_r' = -\frac{\tilde{r}}{2\tilde{\xi}}(ae^{\tilde{z}/\tilde{\xi}} - be^{-\tilde{z}/\tilde{\xi}} - a + b), \tag{D4}$$

with pressure fields similar to those in Appendix C,

$$\tilde{p} = -\tfrac{3}{2}\alpha(\tilde{r}^2 - \tilde{R}^2) + 3\alpha(\tilde{z}^2 - 1) - 6\alpha(\tilde{z} - 1), \tag{D5}$$

$$\tilde{p}' = -\frac{a-b}{4\tilde{\xi}^3}(\tilde{r}^2 - \tilde{R}^2) + \frac{1}{\tilde{\xi}^2}\left\{\frac{a-b}{2\tilde{\xi}}\tilde{z}^2 + \left(a + b - \frac{1}{2}\right)\tilde{z}\right\} + \text{const}. \tag{D6}$$

The coefficients in Eqs. (D1) and (D2) are obtained by matching velocity, tangential velocity, and pressure (at $\tilde{z} = \tilde{L}$), and solving the resulting equations gives an expression

for α that is similar to that in Appendix C. Taking the limiting case when $\exp(L/\xi) \gg 1$ we obtain a simplified expression for α,

$$\alpha = -\frac{\tilde{\xi} e^{\tilde{L}/\tilde{\xi}}}{2 \det[\mathbf{N}]}, \tag{D7}$$

where

$$\mathbf{N} = \begin{pmatrix} e^{\tilde{L}/\tilde{\xi}}(\tilde{L}^3 - 3\tilde{L}^2 + 2 + 6\tilde{\xi}^2 - 6\tilde{\xi}^3) & e^{\tilde{L}/\tilde{\xi}}(\tilde{L} - 1) \\ -3\tilde{\xi}(\tilde{L}^2 - 2\tilde{L} - 2\tilde{\xi}\tilde{L} + 2\tilde{\xi} + 2\tilde{\xi}^2) & -\tilde{\xi} \end{pmatrix}. \tag{D8}$$

Evaluating the matrix determinant gives an expression for α in terms of $\tilde{h} = 1 - 2L/H$ and $\tilde{\xi} = \xi/H$:

$$\alpha = \frac{2}{(\tilde{h} + 2\tilde{\xi})^3 f(\tilde{h}, \tilde{\xi})}, \tag{D9}$$

where

$$f(\tilde{h}, \tilde{\xi}) = 1 + (3\tilde{\xi}^{-1} - 4)x^3 \tag{D10}$$

and $x = 2\tilde{\xi}/(\tilde{h} + 2\tilde{\xi})$. The expression for the single coated surface is qualitatively the same, taking into account the different scaled gaps between the plates,

$$f(\tilde{h}, \tilde{\xi}) = 1 - x'^2 + (12\tilde{\xi}^{-1} - 16)x'^3 - 2x'^4, \tag{D11}$$

where $x' = \tilde{\xi}/(\tilde{h} + \tilde{\xi})$, and $\tilde{h} = 1 - L/H$.

[1] I. Krieger, "Rheology of monodisperse lattices," Adv. Colloid Interface Sci. **3**, 111 (1972).
[2] G. Bossis and J. Brady, "The rheology of Brownian suspensions," J. Chem. Phys. **91**, 1866 (1989).
[3] J. F. Brady and G. Bossis, "The rheology of concentrated suspensions of spheres in simple shear flow by numerical simulation," J. Fluid Mech. **155**, 105 (1985).
[4] J. Brady and J. Morris, "Microstructure of strongly sheared suspensions and its impact on rheology and diffusion," J. Fluid Mech. **348**, 103 (1997).
[5] D. Foss and J. F. Brady, "Structure, diffusion and rheology of Brownian suspensions by Stokesian dynamics simulation," J. Fluid Mech. **407**, 167 (2000).
[6] J. van der Werff, C. de Kruif, C. Blom, and J. Mellema, "Linear viscoelastic behavior of dense hard-sphere dispersions," Phys. Rev. A **39**, 795 (1989).
[7] G. H. Fredrickson and P. Pincus, "Drainage of compressed polymer layers: Dynamics of a squeezed sponge," Langmuir **7**, 786 (1991).
[8] P. S. Doyle, E. S. G. Shaqfeh, and A. P. Gast, "Rheology of polymer brushes: A Brownian dynamics study," Macromolecules **31**, 5474 (1998).
[9] P. De Gennes, *Scaling Concepts in Polymer Physics* (Cornell University Press, New York, 1979).
[10] D. Richter, K. Binder, B. Ewen, and B. Stühn, "Screening of hydrodynamic interactions in dense polymer solutions: A phenomenological theory and neutron-scattering investigations," J. Phys. Chem. **88**, 6618 (1984).
[11] A. Y. Grosberg and A. R. Khokhlov, *Statistical Physics of Macromolecules* (American Institute of Physics, New York, 1994).
[12] P. Ahlrichs, R. Everaers, and B. Dünweg, in *Computer Simulation Studies in Condensed Matter Physics XIV*, edited by D. P. Landau, S. P. Lewis, and H.-B. Schttler (Springer-Verlag, New York, 2001).
[13] P. Ahlrichs, R. Everaers, and B. Dünweg, "Screening of hydrodynamic interactions in semidilute polymer solutions: A computer simulation study," Phys. Rev. E **64**, 040501 (2001).
[14] J. Martin, "Configurational diffusion in semidilute solutions," Macromolecules **19**, 1278 (1986).
[15] P. G. De Gennes, "Dynamic of entangled polymer solutions," Macromolecules **9**, 587 (1976).
[16] H. Brinkman, "A calculation of the viscous force exerted by a flowing fluid on a dense swarm of particles," Appl. Sci. Res., Sect. A **1**, 27 (1947).
[17] D. L. Koch and J. F. Brady, "The effective diffusivity of fibrous media," AICHe J. **32**, 575 (1986).
[18] G. S. Beavers and D. D. Joseph, "Boundary conditions at a naturally permeable wall," J. Fluid Mech. **30**, 197 (1967).
[19] R. E. Larsen and J. J. L. Higdon, "Microscopic flow near the surface of two-phase porous media. Part 1. Axial flow," J. Fluid Mech. **166**, 449 (1986).
[20] R. E. Larsen and J. J. L. Higdon, "Microscopic flow near the surface of two-dimensional porous media. Part 2. Transverse flow," J. Fluid Mech. **178**, 119 (1987).
[21] A. J. C. Ladd, "Hydrodynamics tranasport coefficients of random dispersions of hard spheres," J. Chem. Phys. **93**, 3484 (1990).
[22] A. J. C. Ladd, "Numerical simulations of particulate suspensions via a discretized Boltzmann equation. Part 2. Numerical results," J. Fluid Mech. **271**, 285 (1994).
[23] C. W. J. Beenakker and P. Mazur, "Self-diffusion of spheres in a concentrated suspension," Physica A **120**, 388 (1983).
[24] G. R. McNamara and B. J. Alder, "Analysis of the lattice Boltzmann treatment of hydrodynamics," Physica A **194**, 218 (1993).
[25] A. J. C. Ladd, "Numerical simulations of particulate suspensions via a discretized Boltzmann equation. Part 1. Theoretical foundation," J. Fluid Mech. **271**, 285 (1994).
[26] A. Potanin and W. Russel, "Hydrodynamic interaction of particles with grafted polymer brushes and applications to rheology of colloidal dispersions," Phys. Rev. E **52**, 730 (1995).
[27] J. Klein, Y. Kamiyama, H. Yoshizawa, J. Israelachvili, G. Fredrickson, P. Pincus, and L. Fetters, "Lubrication forces between surfaces bearing polymer brush," Macromolecules **26**, 5552 (1993).
[28] J. Klein, "Shear of polymer brushes," Colloids Surf., A **86**, 63 (1994).
[29] M. A. C. Stuart, F. H. W. H. Waajen, T. Cosgrove, B. Vincent, and T. L. Crowley, "Hydrodynamic thickness of adsorbed polymer layers," Macromolecules **17**, 1825 (1984).
[30] Z. Priel and A. Silberberg, "The thickness of adsorbed polymer layers at a liquid-solid interface as a function of bulk concentration," J. Polym. Sci., Polym. Phys. Ed. **16**, 1917 (1978).
[31] M. Garvey, T. F. Tadros, and B. Vincent, "A comparison of the adsorbed layer thickness obtained by several techniques of various molecular weight fractions of poly (vinyl alcohol) on aqueous polystyrene latex particles," J. Colloid Interface Sci. **55**, 440 (1976).
[32] T. Kato, K. Nakamura, M. Kawaguchi, and A. Takahashi, "Quasielastic light scattering measurements of polystyrene lattices and conformation of poly(oxyethylene) adsorbed on the lattices," Polymer **13**, 1037 (1981).
[33] S. Milner, "Hydrodynamic penetration into the parabolic brushes," Macromolecules **24**, 3704 (1991).
[34] M. Denn, *Process Fluid Mechanics* (Prentice Hall, New York, 1980).